Biochimica et Biophysica Acta 1838 (2014) 2555–2567

Contents lists available at ScienceDirect

Biochimica et Biophysica Acta

journal homepage: www.elsevier.com/locate/bbamem

Structural dynamics and physicochemical properties of pDNA/DODAB: MO lipoplexes: Effect of pH and anionic lipids in inverted non-lamellar phases versus lamellar phases

J.P. Neves Silva [a], I.M.S.C. Oliveira [a], A.C.N. Oliveira [a,b], M. Lúcio [a], A.C. Gomes [b], P.J.G. Coutinho [a], M.E.C.D. Real Oliveira [a,*]

[a] CFUM (Centre of Physics of the University of Minho), Department of Physics, University of Minho, Campus of Gualtar, 4710-057 Braga, Portugal
[b] CBMA (Centre of Molecular and Environmental Biology), Department of Biology, University of Minho, Campus of Gualtar, 4710-057 Braga, Portugal

ARTICLE INFO

Article history:
Received 7 March 2014
Received in revised form 17 June 2014
Accepted 18 June 2014
Available online 27 June 2014

Keywords:
Lipoplexes
Nile Red
FRET
Light scattering
Cryo-TEM
Transfection

ABSTRACT

Dioctadecyldimethylammonium bromide (DODAB):Monoolein (MO) lipoplexes have mainly been studied within the range of high molar ratios of DODAB, with noticeable transfection efficiencies in the Human Embryonic Kidney (HEK, a.k.a. 293T) cell line. In this work, we intend to study the effect of high MO content on the structure and physicochemical properties of pDNA/DODAB:MO lipoplexes to achieve some correlation with their transfection efficiency. Static/Dynamic Light Scattering and Cryo-TEM imaging were used to characterize the size/morphology of DNA/DODAB:MO lipoplexes at different DODAB:MO contents (2:1, 1:1, 1:2) and charge ratios (CRs) (+/−). Nile Red fluorescence emission was performed to detect changes in microviscosity, hydration and polarity of DNA/DODAB:MO systems. Lipoplexes stability at physiological pH values and in the presence of anionic lipids was evaluated by Förster Resonance Energy Transfer (FRET). Physicochemical/structural data were complemented with transfection studies in HEK cells using the β-galactosidase reporter gene activity assay. This work reports the coexistence of multilamellar and non-lamellar inverted phases in MO-richer lipoplexes (DODAB:MO 1:2 and 1:4), leading to transfection efficiencies comparable to those of multilamellar (DODAB-richer) lipoplexes, but at higher charge ratios [CR (+/−) = 6.0] and without dose-effect response. These results may be related to the structural changes of lipoplexes promoted by high MO content.

1. Introduction

The progress of gene therapy in the last few decades has been achieved mostly through the development of stable carriers, capable of condensing genetic material and withstanding the harsh destabilizing conditions of the biological environment [1–8]. Although having attained high rates of cell internalization, these carriers have limited release of genetic material into the cytoplasm, which explains their relatively low cell transfection efficiency [9,10]. For the particular case of liposome-based carriers, the inclusion of non-lamellar forming lipids (also called *helper* lipids) in the liposomal formulations has been one of the strategies chosen to overcome this problem. This approach potentiates the formation of membrane fusion intermediates that disrupt the lamellar organization of cationic liposome/DNA complexes (lipoplexes), and favor the release of its genetic content [11,12]. Molecules such as dioleoylphosphatidyl ethanolamine (DOPE) and cholesterol (Chol) have been employed as successful *helper* lipids in several liposomal formulations, enhancing the lipofection efficiency through the formation of inverted hexagonal structures (H_{II}) [7,13–15]. Equimolar proportions of cationic and *helper* lipids are required to develop lamellar-structured lipoplexes that are capable of transitioning to an inverted hexagonal phase upon pH decrease during endocytosis, thus favoring the destabilization of the endosomal membrane and the release of the genetic material into the cytoplasm [16].

Recent studies have associated synthetic tensioactives, such as 1,2-dioleoyl-*sn*-glycero-3-hexylphosphocholine (C6-DOPC) and 1,2-dierucoyl-*sn*-glycero-3-ethylphosphocholine (di22:1-EPC), and the natural surfactant Monoolein (MO), with the formation of inverted mesophases in cationic lipoplexes [17–20]. The enhancement in cell transfection efficiency observed for formulations based on these type of surfactants has been correlated with the promotion of inter-lamellar attachments (ILAs) and packing defects, that destabilizes the lamellar arrangement of cationic lipoplexes and favors nucleic acid release from the lipoplex structure upon membrane fusion [21,22]. For the nucleic acid (NA)/cationic liposome formulation composed by the synthetic cationic lipid dioctadecyldimethylammonium bromide (DODAB) and the non-ionic and non-lamellar forming lipid MO, the appearance of such non-lamellar inverted mesophases seems to only occur at equimolar or exceeding molar fractions of the *helper* lipid MO

* Corresponding author. Tel.: +351 253 604 325; fax: +351 253 678 981.
E-mail address: beta@fisica.uminho.pt (M.E.C.D.R. Oliveira).

http://dx.doi.org/10.1016/j.bbamem.2014.06.014
0005-2736/

[23]. Nevertheless, the system has only been studied until now for exceeding molar fractions of DODAB, where a multilamellar organization is predominant [23]. In this work, we studied the behavior of pDNA/DODAB:MO lipoplexes at high MO contents (1:2 and 1:4 DODAB:MO ratios), where inverted bicontinuous non-lamellar phases are more likely to form and remain stabilized [24]. The physicochemical properties, destabilization dynamics and transfection efficiency of the mixtures were determined and compared with DNA/DODAB:MO (2:1) lipoplexes (multilamellar organization).

Nile Red fluorescence emission and anisotropy were used to detect variations in the microviscosity, hydration and polarity of these systems, eventually caused by the presence of MO and/or DNA in the lipoplexes. The hydrophobic nature of this fluorescent probe and the strong dependence of its steady-state emission with the local microenvironment where it is located have already been used in the physicochemical characterization of several lipid mixtures, including DODAB:MO aggregates in the absence of DNA [25]. Another fluorescence technique, specifically FRET, was used to monitor conformational changes in the structure of DNA/DODAB:MO lipoplexes upon charge ratio (+/−) increase and MO content variation. The chosen acceptor/donor pair of fluorescent probes BOBO-1 and Rhodamine-DHPE was also employed to observe the effects of pH decrease and interaction with anionic/neutral lipids on the DNA compaction within the lipoplexes. These are two of the main factors involved in lipoplex degradation during endosomal escape, which is a strong limitation for the transfection efficiency of the lipoplexes.

Fluorescence spectroscopy data was complemented with 90° Static Light Scattering (90° SLS), Dynamic Light Scattering (DLS) and cryo-Transmission Electron Microscopy (cryo-TEM), in order to analyze the reorganization of the structure during lipoplex formation and destabilization, with special emphasis to the inverted non-lamellar phases of pDNA/DODAB:MO (1:2 and 1:4) formulations. Finally, the transfection efficiency of DNA/DODAB:MO lipoplexes (2:1, 1:1, 1:2, 1:4) on the Human Embryonic Kidney (HEK) 293T cell line was correlated with the structure of the lipoplexes.

2. Materials and methods

2.1. Reagents

The lipid surfactants 1-monoolein (MO) and dioctadecyldimethylammonium bromide (DODAB) were purchased, respectively, from Sigma-Aldrich and Tokyo-Kasei. The tensioactives oleic acid (OA), dioleoylphosphatidic acid (DOPA), dioleoylphosphatidylglycerol (DOPG) and dioleoylphosphatidylethanolamine (DOPE) were purchased from Avanti Polar Lipids. The solvatochromic/anisotropy probe 9-(diethylamino)-5H-benzo[a]phenoxazin-5-one (Nile Red), the lipid probe triethylammonium 5-(N-(2-(((2,3-bis(palmitoyloxy) propoxy)oxidophosphoryl)oxy)ethyl)sulfamoyl)-2-(6-(diethylamino)-3-(diethyliminio)-3H-xanthen-9-yl)benzenesulfonate (Rhodamine-DHPE) and the DNA intercalating probe 2,2′-((1,1′-((propane-1,3-diylbis(dimethylammonionediyl))bis(propane-3,1-diyl))bis(pyridin-1(1H)-yl-4(1H)-ylidene))bis(methanylylidene))bis(3-methylbenzo[d] thiazol-3-ium) iodide (BOBO-1) were purchased from Sigma-Aldrich. Salmon sperm DNA was purchased from Invitrogen. All reagents were used in the same conditions as received. The surfactant molecules used in this study are shown in Fig. 1.

2.2. Liposome preparation

For fluorimetric assays involving either Nile Red (fluorescence anisotropy) or Rhodamine-DHPE (FRET), predefined volumes of the probes were first transferred to an Eppendorf. The solvent was evaporated under a nitrogen steam, originating a probe film that was resolubilized with the appropriate volume of DODAB and MO (20 mM stock solutions in ethanol). The final ratio probe/lipid (mol/mol) for Nile Red and Rhodamine DHPE was kept, respectively, to 1:500 and 1:200.

The lipid solutions (either with or without the fluorescence probes) were injected under vigorous vortex to an aqueous buffer solution of Tris-HCl (30 mM) at 70 °C. Liposome solutions with a final lipid concentration ([DODAB:MO]) of 1 mM and different DODAB:MO molar ratios: 2:1, 1:1, 1:2 and 1:4 were produced.

2.3. Lipoplex preparation

Lipoplexes were prepared by adding the DODAB:MO cationic liposomes in an instant-mixing procedure (25 °C) to a DNA buffered solution (20 μM). The time duration of the lipoplex formation procedure depended on the type of physicochemical characterization technique that was used. For DLS, 90° SLS, Zeta Potential and Cryo-TEM assays, the lipoplex incubation period was set to 30 min. For fluorometric experiments involving either FRET or Nile Red Fluorescence, the stabilization time for each data point involved in the same experiment was 5 min, so that the final incubation period was equal to the cumulated time of all consecutive data points. The lipoplexes were generated with ammonium/phosphate charge ratios (CRs) (+/−) between 0.0 and 4.0. The concentration of nucleotide bases (determined by the DNA absorption at wavelength 260 nm [26]), was held constant at 4.2×10^{-5} M in all experiments.

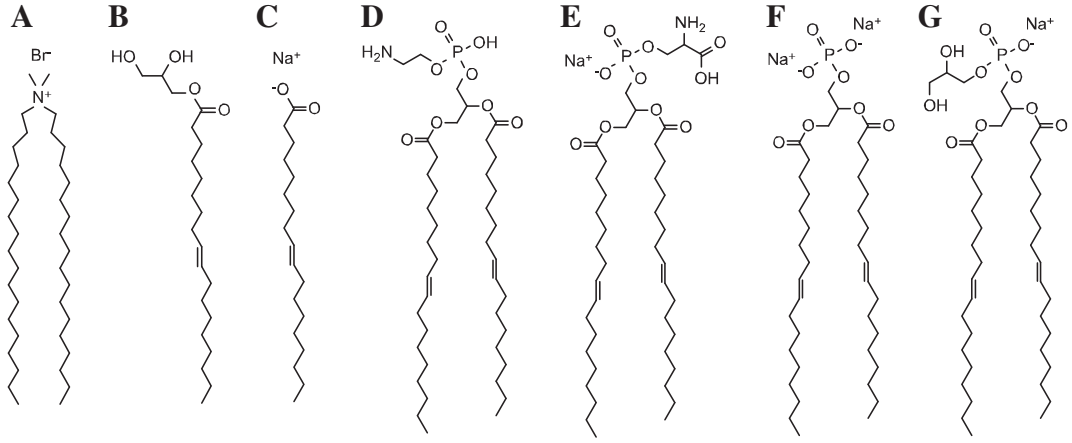

Fig. 1. Molecular structures of the lipids used in this study. A) Dioctadecyldimethylammonium bromide (DODAB); B) 1-Monoolein (MO); C) Oleic Acid (OA); D) Dioleoylphosphatidylethanolamine (DOPE); E) Dioleoylphosphatidylserine (DOPS); F) Dioleoylphosphatidic Acid (DOPA); G) Dioleoylphosphatidylglycerol (DOPG).

2.4. Lipoplex destabilization

In vitro simulation of the main factors involved in DNA/DODAB:MO lipoplex degradation during endosomal escape process was performed by FRET analysis, upon the addition of different anionic/neutral lipids to lipoplexes and also through the acidification of a non-buffered aqueous solution of lipoplexes with HCl. For anionic/neutral lipid addition, DOPG:DOPA (1:1), DOPG:DOPS (1:1), DOPG:DOPE (1:1) and DOPG:OA (1:1) lipid aggregates (from now on, termed DOPA, DOPS, DOPE and OA aggregates, respectively, for a matter of simplification) were prepared by ethanol injection method. The lipid aggregates were then progressively added to DNA/DODAB:MO labeled lipoplexes (see section 2.6) at CR (+/−) = 4.0 in Tris-HCl (30 mM), until a final lipid concentration of approximately 200 μM. For the pH acidification assay, the labeled lipoplexes were first prepared at the same CR (+/−) = 4.0 in ultrapure water, and then titrated with HCl (1 mM).

2.5. Nile Red fluorescence emission and anisotropy assays

It is known that the maximum wavelength of Nile Red emission spectrum increases with the polarity of the environment [27]. Additionally, Nile Red fluorescence lifetime decreases with the increase of the hydrogen bonding capability of the medium [28]. For Nile Red assays, 2500 μL of salmon sperm DNA solution (20 μM) was placed in a cuvette and then incubated for 5 min, under agitation, with defined volumes of the liposomal mixtures with Nile Red, to obtain the intended ammonium/phosphate charge ratio CR (+/−). The polarized emission spectra for Nile Red were then recorded in a Horiba Jobin Yvon Spex Fluorolog 3 spectrofluorometer using Spex polarizers with λ_{exc} at 525 nm. All spectra were corrected for the instrumental response of the system, and the solvent background was subtracted.

A two-state model for excited state behavior of Nile Red involving a solvent relaxation process, where A* and B* represent the initially excited and the relaxed excited state, with the possibility of a reversible reaction (Khrishna model [27]) was assumed:

$$A^* \underset{k_{BA}}{\overset{k_{AB}}{\rightleftarrows}} B^* \quad \searrow \textit{Ground State} \swarrow \tag{1}$$

The emission spectra of Nile Red were obtained from anisotropy measurements [29]:

$$I_{total} = I_{VV} + (2 \cdot G \cdot I_{VH}) \tag{2}$$

where G, equivalent to the ratio I_{HV}/I_{HH}, is the internal correction factor for the sensitivity of the spectrofluorometer for vertically (V) and horizontally (H) polarized light. The corresponding anisotropy spectra are given by:

$$r(\lambda) = \frac{I_{VV} - G.I_{VH}}{I_{VV} + 2.G.I_{VH}} \tag{3}$$

(I_{VV}) and $(G \times I_{VH})$ were simultaneously fitted to a sum of two lognormal functions [29]:

$$I_{VV/VH} = \frac{\left(A_{VV/VH}\right)_1}{(\lambda - (\lambda_{max})_1 + a)} \cdot exp\left(-c^2\right) \cdot exp\left\{-\frac{1}{2 \cdot c^2} \cdot \left[ln\left(\frac{\lambda - (\lambda_{max})_1 + a}{b}\right)\right]^2\right\} + \frac{\left(A_{VV/VH}\right)_2}{(\lambda - (\lambda_{max})_2 + a)} \cdot exp\left(-c^2\right) \cdot exp\left\{-\frac{1}{2 \cdot c^2} \cdot \left[ln\left(\frac{\lambda - (\lambda_{max})_2 + a}{b}\right)\right]^2\right\} \tag{4}$$

where A is the maximum emission intensity at λ_{max}, and the parameters a, b and c are given by [29]:

$$a = H \cdot \frac{\rho}{\rho^2 - 1} \tag{5}$$

$$b = H \cdot \frac{\rho}{\rho^2 - 1} \cdot exp\left(c^2\right) \tag{6}$$

$$c = \frac{\ln(\rho)}{\sqrt{2 \cdot \ln(2)}} \tag{7}$$

where, H and ρ are, respectively, the halfwidth and skewness of the band. Only the parameters with *VV* or *HH* subscript depend on whether (I_{VV}) or $(G \times I_{VH})$ spectra are being fitted. The steady-state fluorescence anisotropies of initially excited state (r_1) and solvent relaxed state (r_2), as well as the emission intensity fraction of the initially excited state (f_1) are given by [29]:

$$r_1 = \frac{(A_{VV})_1 - (A_{VH})_1}{(A_{VV})_1 + 2 \cdot (A_{VH})_1} \tag{8}$$

$$r_2 = \frac{(A_{VV})_2 - (A_{VH})_2}{(A_{VV})_2 + 2 \cdot (A_{VH})_2} \tag{9}$$

$$f_1 = \frac{(A_{VV})_1 + 2 \cdot (A_{VH})_1}{(A_{VV})_1 + 2 \cdot (A_{VH})_1 + (A_{VV})_2 + 2 \cdot (A_{VH})_2}. \tag{10}$$

2.6. Förster resonance energy transfer (FRET) assays

Förster resonance energy transfer (FRET) is a non-radiative transfer process of the excitation energy from a donor to an acceptor chromophore, that is mediated by a long-range dipole–dipole interactions (Förster) [30]. The Förster resonance energy transfer efficiency (Φ_{FRET}) is given by the following equation [31]:

$$\phi_{FRET} = \frac{1}{1 + (r_{DA}/R_o)^6} \tag{11}$$

where (R_o) is the critical radius of Förster at which the energy transfer and the spontaneous decay of the excited donor are equally probable (50%), and (r_{DA}) is the distance between donor and acceptor species [31]. For the FRET assays performed in this study, 2500 μL of salmon sperm DNA solution at 25°C (20 μg/μL) labeled with BOBO-1 (ratio probe/phosphate = 1/100 mol/mol) was added to a cuvette and then incubated for 5 min, with agitation, with defined volumes of the appropriate liposomal mixtures containing rhodamine-DHPE (ratio probe/lipid = 1/200 mol/mol), to obtain the intended ammonium/phosphate charge ratio CR (+/−). The fluorescence emission spectra (470–700 nm) were then recorded in a Horiba Jobin Yvon Spex Fluorolog 3 spectrofluorometer with λ_{exc} of 460 nm. All spectra were corrected for the instrumental response of the system, and the solvent background was subtracted. The Förster resonance energy transfer efficiency (Φ_{FRET}) was determined through the following equation:

$$\Phi_{FRET} = 1 - \frac{\Phi_D}{\Phi_D^0} = 1 - \frac{A(\lambda_D)}{A_D(\lambda_D)} \frac{I_D(\lambda_D, \lambda_D^{em})}{I_D^0(\lambda_D, \lambda_D^{em})} \tag{12}$$

where $(\Phi_D{}^0)$ and (Φ_D) are the donor quantum yields in the absence and presence of acceptor, respectively. Eq. (12) is valid when there is negligible emission from the acceptor. In the assays performed with the donor/acceptor pair BOBO-1/rhodamine DHPE, the factor $[A(\lambda_D) / A_D(\lambda_D)]$ has been considered equivalent to 1 due to its neglectable

contribution to the overall absorption at the excitation wavelength (λ_D) (see Supplementary material 1). After the determination of (Φ_{FRET}) through Eq. (12), this parameter was followed upon the destabilization of DNA/DODAB:MO CR (+/−) = 4.0 lipoplexes by pH decrease and neutral/anionic lipid addition.

2.7. 90° Static light scattering (90° SLS) assays

The 90° SLS assays were performed for all CRs (+/−) in a Horiba Jobin Yvon Spex Fluorolog 3 spectrofluorometer, with the scattering intensities being recorded in timescans of 60 s each, with excitation and emission monochromators set respectively to 600 and 601 nm, at which there is neither absorbance, nor fluorescence emission.

2.8. Dynamic light scattering (DLS) assays

DNA/DODAB:MO lipoplexes with different MO contents (2:1, 1:1, and 1:2) were prepared at charge ratios CR (+/−) = 0.25, 0.5, 0.75, 1.0, 1.5, 2.0 and 4.0 and placed in disposable polystyrene cuvettes for DLS measurements in a Malvern Zetasizer Nano ZS particle analyzer. Malvern Dispersion Technology Software (DTS) was used with multiple narrow mode (high resolution) data processing, enabling the recovery of the mean size (nm) and associated error values.

2.9. Cryo-TEM assays

For cryo-TEM studies, cryo-TEM grids were prepared following standard procedures. 3 μL of lipoplexes at 1.2 mg/mL in Tris-HCl buffer solution (pH 7.4) was placed onto 200-mesh holey EM grids and vitrified in liquid ethane at liquid nitrogen temperature using a Vitrobot (FEI). Cryo-TEM grids were observed at liquid nitrogen temperature on a FEG JEM2200-FS/CR transmission electron microscope (JEOL) operated at 200 kV. Digital images were recorded on a 4 K × 4 K CCD camera Ultrascan4000™ (GATAN) under low-dose conditions and using DigitalMicrograph™ (GATAN) software in binned mode. An in-column omega energy filter helped to record images with improved signal to noise ratio by zero-loss filtering. The energy selecting slit width was set at 9 eV. The images presented here were taken using the nominal magnification of 50,000 resulting in a final pixel size of 4.3 Å with a defocus value ranging from −3 to −1 μm. The total electron doses were on the order of 7–20 electrons/Å^2.

2.10. Cell culture and transfection assays

The 293T cell line was cultured in DMEM complete growth medium (10% (v/v) heat-inactivated FBS and penicillin/streptomycin/amphotericin B (10,000 units/10 mg/25 μg per mL)), and cells were sub-cultured every two days in order to maintain sub-confluency.

293T cells were seeded into 24-well plates and incubated overnight at 37 °C, 5% CO_2. Immediately before transfection, the cell culture medium was replaced and 100 μL of the lipoplex solutions (DODAB:MO 2:1, 1:1, 1:2 and 1:4) was added to each well. After a 48 h period of incubation, β-galactosidase activity was evaluated with the β-Galactosidase Enzyme Assay System with Reporter Lysis Buffer, according to the standard protocol [32]. Lipofectamine™ LTX Reagent was used as a control, according to manufacturer's instructions. Data from three independent experiments were considered to identify differences across the various formulations.

3. Results & discussion

3.1. Microviscosity/hydration changes of DODAB:MO formulations with different MO content and upon the presence of DNA

Nile Red is a hydrophobic and solvatochromic probe that presents a well-known dependence of its steady-state emission properties with the polarity and the hydration level of the medium [29,33]. This probe usually exhibits an increase in fluorescence yield with decreasing solvent polarity, with a corresponding blue shift in the peak emission [27]. Moreover, the fluorescence lifetime of Nile Red decreases with the increase of H-bonding capability of the medium [28], thus reporting on the level of hydration of the membrane. Therefore, this probe was selected to report the influence of both the presence of DNA and an increasing content of MO in the physicochemical properties of DNA/DODAB:MO lipoplexes (such as microviscosity, hydration and polarity) and also to achieve some correlation between the lipoplex physicochemical properties and their transfection efficiency [19]. Fig. 2 shows the total fluorescence intensity of Nile Red normalized to lipid concentration on DNA/DODAB:MO (2:1, 1:1 and 1:2) lipoplexes as a function of CR (+/−).

As the probe:lipid molar ratio was kept constant at a value of 1:500 (mol:mol), it was expected that Nile Red fluorescence would be constant when divided by concentration. However, at low CR (+/−) (<0.6), variations in Nile Red fluorescence emission were observed, suggesting structural changes of the aggregates dependent on the total lipid concentration and on DODAB:MO molar ratio. This may be explained by the presence of pre-vesicular structures at low lipid concentrations, as already detected on mixtures of DODAB and MO in the absence of DNA [25]. In fact, when Nile Red fluorescence emission in the DODAB:MO lipoplexes (with DNA) is divided by Nile Red fluorescence emission in the DODAB:MO aggregates (without DNA) (Fig. 2B), the fluorescence emission remains constant, only exhibiting a peaked behavior around CR (+/−) = 1.0 for the system DODAB:MO (1:1), and around CR (+/−) = 1.3 for DODAB/MO (1:2), being absent in the system with less MO content (2:1). This peaked behavior occurs near the neutralization point of lipoplex assembly, and corresponds to the extensive lipid mixing that triggers the appearance of highly organized structures (sandwich-type, hexagonal or inverted bicontinuous cubic structures) with different levels of hydration and polarity [8,20,34].

The emission spectra of Nile Red in DNA/DODAB:MO systems with different molar ratios (2:1, 1:1 and 1:2) and four different CRs (+/−) (A = 0.20; B = 0.50; C = 1.00; and D = 2.00) are represented in Fig. 3.

An increase in fluorescence emission with MO content for all charge ratios is observable in Fig. 3. This variation, seen for CRs (+/−) up to 0.5, is the same as previously observed for DODAB:MO systems in the absence of DNA and with low MO content [25]. The observed increase in fluorescence emission of Nile Red points to a decrease in hydration, possibly due to a reduction in the contact between the probe and the aqueous surrounding, thus suggesting closer contact between the probe and inverted non-lamellar phase formed by MO enriched domains enclosed by DODAB bilayers. Moreover, as seen in Fig. 2, the fluorescence intensity of the probe increases with CR (+/−) increase. This can be explained by the DNA coating of liposomes, that results in less hydrated DODAB:MO bilayer structures. The dehydration of both DNA and lipids is an important requirement to obtain a tight contact during their interaction, and a similar decrease in hydration has been reported on the assembly of other lipoplexes [8,35].

A small red spectral shift is also observed for DNA/DODAB:MO (2:1) at CRs (+/−) below 0.5, with the appearance of a blue shoulder on the emission spectra of Nile Red. In the lipid systems without DNA, it was found that the blue shoulder magnitude of the Nile Red spectra increased with the DODAB content, following the order DODAB:MO (0:1) < (1:2) < (1:1) < (2:1) < (1:0). This behavior is related to the fact that the lamellar structures are favored at high DODAB contents, which implies a less polar surrounding environment of the probe [25]. In the presence of DNA, and at comparable lipid concentrations, the structural differences between the mentioned systems are much less pronounced, and above CR (+/−) = 0.5 the spectral shape is constant and the blue shoulder is almost lost. The red shift and the shape of the spectrum for DODAB:MO (2:1) at very small charge ratios suggest

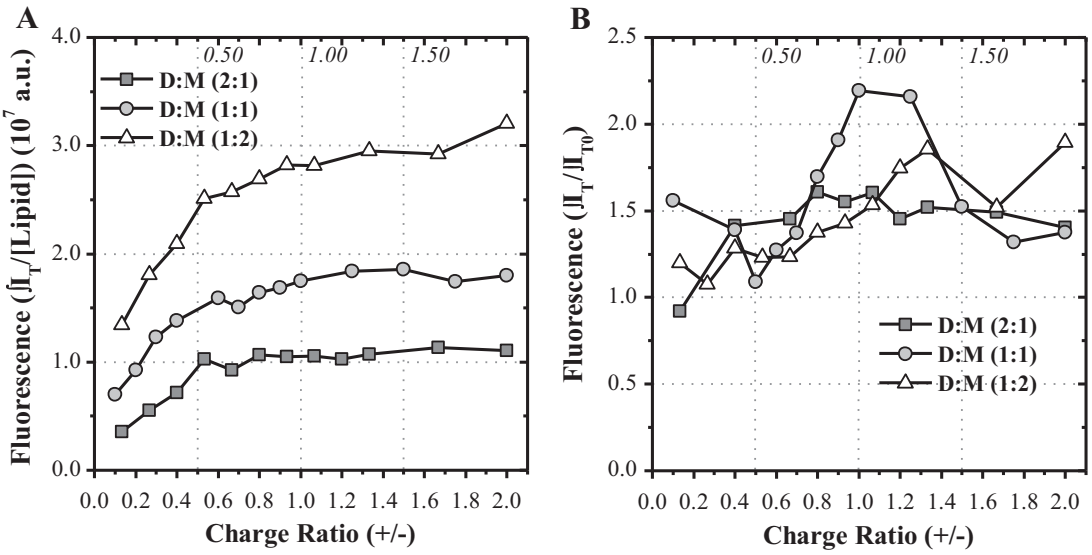

Fig. 2. Variation of the total fluorescence intensities of Nile Red with charge ratio (+/−), for the titration of salmon sperm DNA with different DODAB:MO molar ratios (2:1, 1:1 and 1:2), all represented as a function of total lipid concentration (A) and Nile Red fluorescence emission in the absence of DNA (B).

that, in this case, Nile Red feels an environment similar to DODAB in the gel phase [33]. Since this feature was not observed in the absence of DNA [25], it seems that when MO content is low, DODAB-rich domains are formed upon coating with DNA. These domains disappear either due to increase of lipid content or due to lipoplex restructuring, as can be observed in Fig. 3B and C.

In order to gain further insight on the type of structural changes that occur upon variation on MO content and total lipid concentration, we

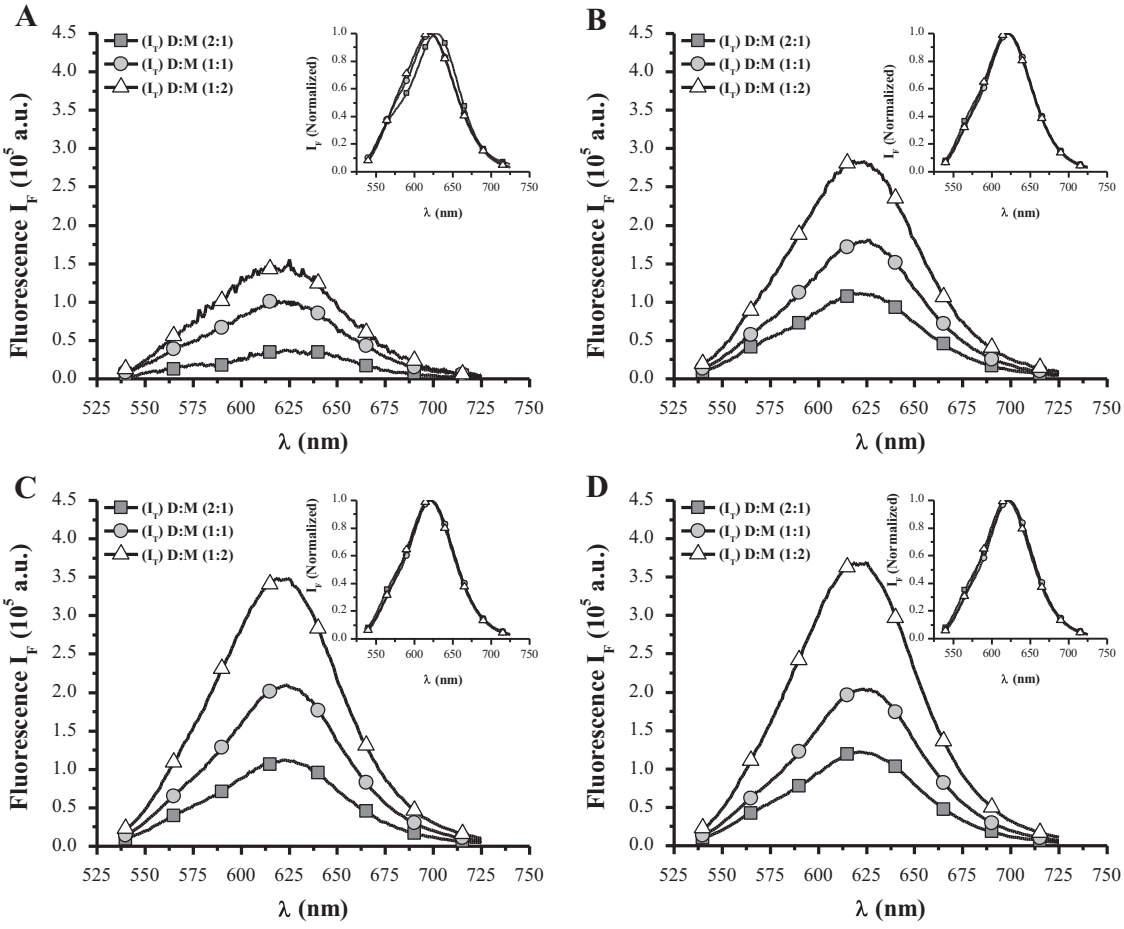

Fig. 3. Fluorescence emission spectra of Nile Red in DNA/DODAB:MO lipoplexes with different DODAB:MO molar ratios (2:1, 1:1 and 1:2) and charge ratios (+/−) (A — 0.20; B — 0.50; C — 1.00; and D — 2.00).

have also studied Nile Red fluorescence anisotropy in DNA/DODAB:MO lipoplexes. Fluidity is an important biophysical parameter to characterize lipid bilayers in the absence and presence of DNA, which is related to the release of the DNA into the mammalian cells [36]. Thus, the ability of a lipid to form stable liposomes (and stable lipoplexes) ought to be regarded along with anisotropy measurements. Fluorescence anisotropy can provide information on the microviscosity/fluidity of the lipoplexes, because as the system becomes more fluid, the degree of rotation of the excited fluorophore placed within the system increases, and, accordingly, the anisotropy decreases. The use of a two-state model gives more localized information through Nile Red solvation cage dynamics. As already mentioned in Section 2.4, this two-state model involves a solvent relaxed excited state (B*) and an initial excited state (A*), but each one of these states can reflect an overlapping of different environments and structures. Supplementary Fig. 2 illustrates, for the DNA/DODAB:MO (1:1) system, the results of Nile Red fluorescence anisotropy modeling, showing the recovered theoretical anisotropies (r_t) with the experimental values (r_e). A good correspondence between the experimental results and theoretical model was also obtained for Nile Red emission spectra reconstructed from anisotropy data (Supplementary Fig. 3), according to Eq. (2).

Fig. 4 represents the recovered theoretical anisotropies for DNA/DODAB:MO lipoplexes with different molar ratios (2:1, 1:1 and 1:2) and four different CRs (+/−) (A = 0.20; B = 0.50; C = 1.00; and D = 2.00).

It is well known that the presence of *helper* lipids induces a decrease in fluorescence anisotropy, reflecting an increase in the fluidity of lipoplexes [36,37]. Similarly, regardless of the charge ratios tested, our results show a general decrease in anisotropy with the increase in MO content, indicating that the probe is located within the more fluid inverted non-lamellar MO domains when the *helper* lipid is present in higher percentages. For CR (+/−) = 0.20 and the lowest MO content in DNA/DODAB:MO (2:1) lipoplexes, a very high anisotropy is observed, probably related to the previously reported formation of non-vesicular structures [25] and also to the formation of the above mentioned DODAB-rich domains. In Fig. 5, the recovered values for r_1, r_2, λ_1, λ_2 and f_1 are plotted as a function of CR (+/−).

For all lipoplexes at CR (+/−) < 0.5, the values for r_1 and r_2 decrease with MO content increase, confirming the more fluid environment of MO domains in the MO rich lipoplexes. Although a decrease in both anisotropy components is observed, this is more evident on the r_2 component. The decrease in r_2 component in DODAB rich lipoplexes, such as DODAB:MO (2:1), is more pronounced than that reported in the absence of DNA in comparable total lipid concentrations (from 0.16 to 0.09) [25]. This is in agreement with a reported DNA fluidization effect on the lipoplexes [37]. It is proposed that, especially at temperatures below phase transition, the interaction of the negatively charged DNA backbone with the cationic lipid head groups can lead to a less tightly

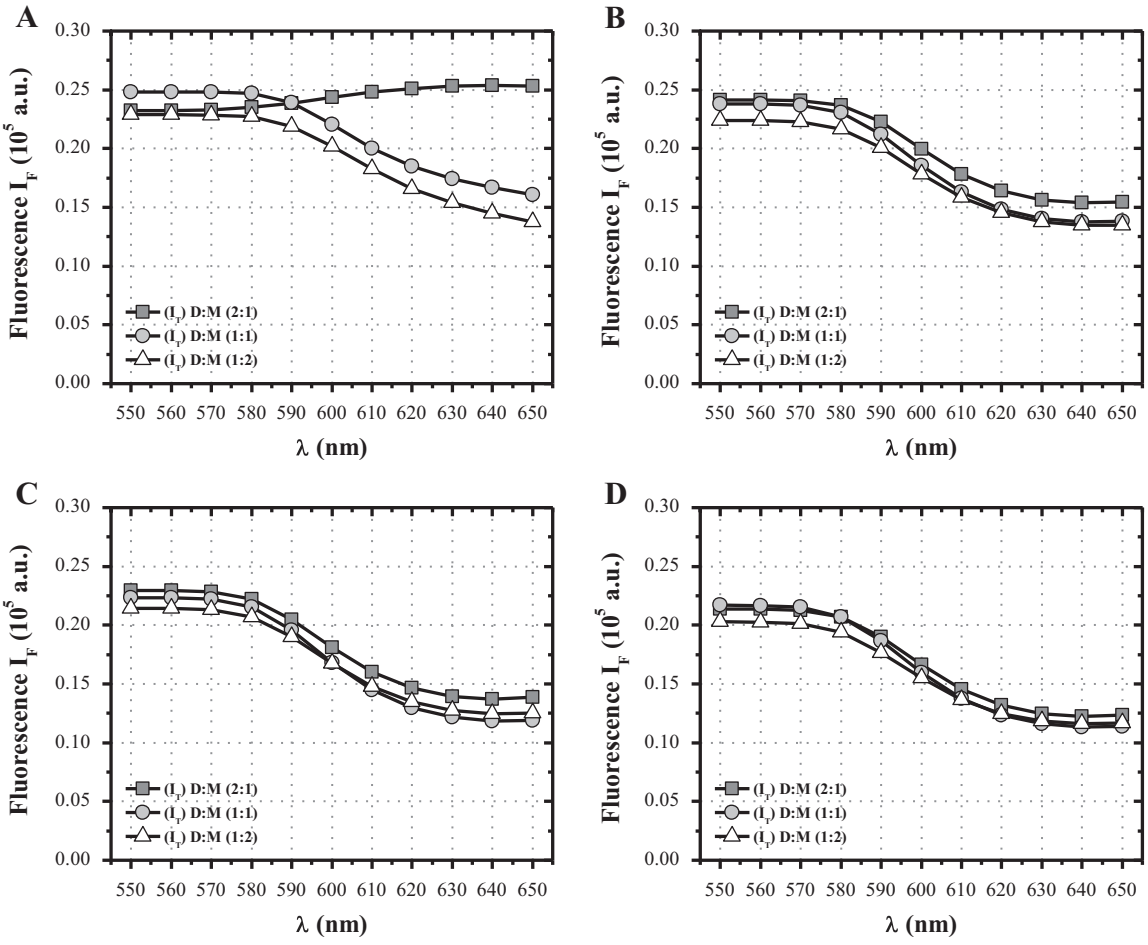

Fig. 4. Variation of theoretical fluorescence anisotropies (r_t) of Nile Red in DNA/DODAB:MO lipoplexes with different DODAB:MO molar ratios (2:1, 1:1 and 1:2) and charge ratios (+/−) (A — 0.20; B — 0.50; C — 1.00; and D — 2.00). Calculated r_t values were determined through the two-state model previously described (Eqs. 3 and 4).

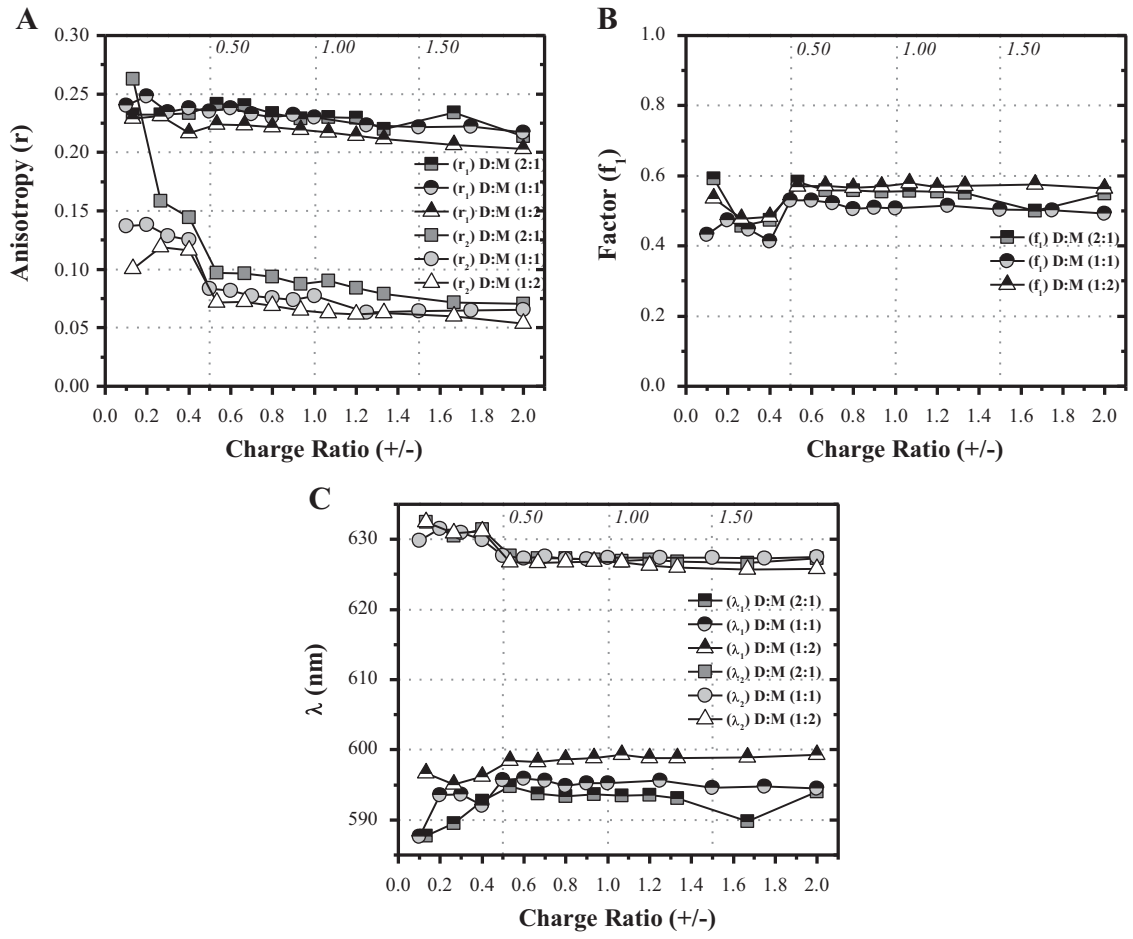

Fig. 5. Variation of recovered Nile Red fluorescence anisotropies (r_1 and r_2) (A), fluorescence distribution factor (f_1) (B), and fluorescence emission wavelengths (λ_1 and λ_2) (C) with DODAB:MO molar fraction (2:1, 1:1 and 1:2), as a function of charge ratio (+/−). Calculated r_1, r_2, f_1, λ_1 and λ_2 values were determined through the two-state model previously described (Eqs. 8–10).

packed lipid structure [37]. Infrared studies also support this theory, and suggest that the alignment of the lipid headgroups with DNA alters the packing of the lipid molecules, increasing the conformational disorder of lipid hydrocarbon tails [38]. Similar results have been reported for other lipoplexes through NMR experiments, where it is shown that DNA–lipid electrostatic interactions reduce the long-range lipid mobility, but locally enhance the hydrocarbon chain dynamics by perturbing the preferred lipid packing [39]. Fig. 5 also shows that, for lipoplexes at CRs (+/−) > 0.5, although not as pronounced as for CRs (+/−) < 0.5, the same trend is observed for r_1, r_2 and f_1, i.e. an anisotropy decrease with the increase of MO content, confirming the more fluid environment felt by Nile Red in the MO-rich lipoplexes.

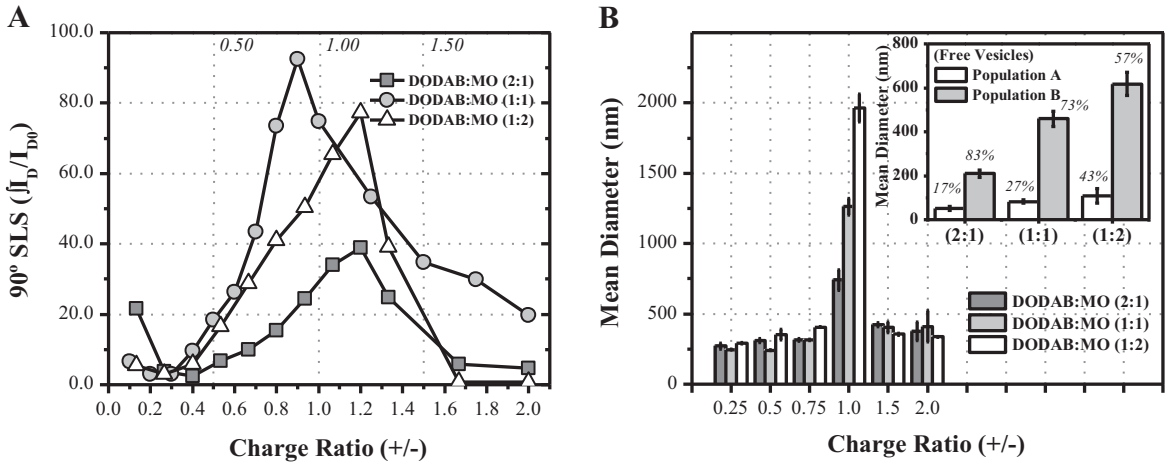

Fig. 6. Variation of 90° Static Light Scattering intensity (A) and mean particle diameter (nm) obtained by Dynamic Light Scattering (B) with charge ratio (+/−), for the titration of salmon sperm DNA with different DODAB:MO molar ratios (2:1, 1:1 and 1:2). Inset in section 6B: Size distribution (nm) of the free DODAB:MO liposomes at the same total lipid concentrations used to attain charge ratio (+/−) 2.0, with the corresponding relative frequency percentages of populations A and B.

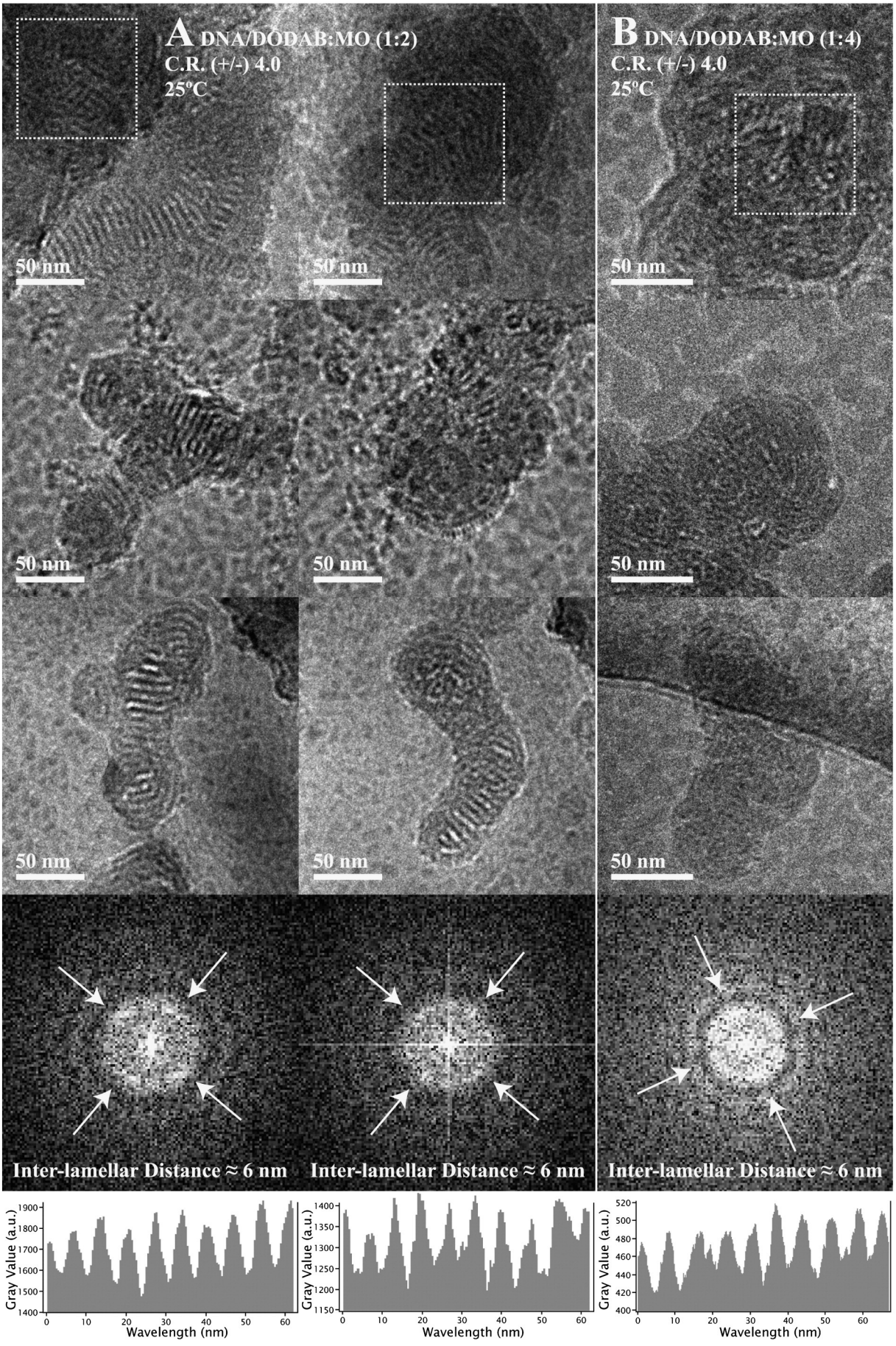
A DNA/DODAB:MO (1:2)
C.R. (+/-) 4.0
25°C
B DNA/DODAB:MO (1:4)
C.R. (+/-) 4.0
25°C
50 nm
Inter-lamellar Distance ≈ 6 nm
Gray Value (a.u.)
Wavelength (nm)

Overall, for the lipoplexes prepared at different CR (+/−), the anisotropy values obtained were less than 0.2–0.3, which are believed to describe structure fluid enough to result in an efficient transfection process [36,37].

The emission wavelength of the initially excited state (λ_1) shows an initial red shift with increasing CRs (+/−), followed by stabilization (Fig. 5). These variations are consistent with the trends shown by the blue shoulder of the emission spectra in Fig. 3, due to the existence of pre-vesicular structures already seen in the absence of DNA [25].

The λ_1 values also show a red shift with increasing MO content, which follows the same trend as observed in the absence of DNA [25]. This indicates that, despite sensing less hydration by being deeper located at the MO domains (as concluded from the increase on the emission intensity in Fig. 3), Nile Red reports a polarity increase with higher MO content, probably by the exposition of the probe to the hydroxyl groups of MO. Nevertheless, all maximum emission wavelengths (λ_1 and λ_2) are blue shifted when compared with corresponding systems without DNA, revealing a more hydrophobic environment sensed by the probe. This is in agreement with the observed increase of Nile Red fluorescence upon DNA interaction, explained by the already mentioned DNA coating effect, which reduces the exposition of the probe to the more hydrated environment. The maximum emission wavelength of the relaxed excited state (λ_2) shows much less dependence on MO content when compared with λ_1. This result was already expected, as the relaxed excited state (λ_2) reports for the relaxed "solvent" cage of Nile Red, which is not so sensitive to MO content.

3.2. The effect of MO content on the structural dynamics of DNA/DODAB:MO lipoplexes

Dynamic Light Scattering (DLS) gives information on the average size of the lipoplexes, while 90° Static Light Scattering (90° SLS) provides information about the structure of the lipoplexes. This information can be obtained when the intensity of scattered light for DNA/DODAB:MO lipoplexes (I_D) is divided by the intensity of scattered light for DODAB:MO aggregates at the equivalent lipid concentration (I_{D0}) [40].

Fig. 6A shows the variation on intensity of static scattered light with CR (+/−), for different DNA/DODAB:MO (2:1, 1:1 and 1:2) lipoplexes. A different scattering behavior is observed for the three systems with the increase of CR (+/−). Fig. 6B presents the particle mean size (nm), determined by Dynamic Light Scattering (DLS), for the same DNA/DODAB:MO lipoplexes. Although at charge neutralization point CR (+/−) = 1.0 the average size of the lipoplexes increases with MO content, after the neutralization point all three formulations present similar sizes, which are comparable to the size of free liposomes (inset of Fig. 6B). It is interesting to note that free liposomes present a bimodal distribution, with an overall general size increase [(f_A·*population A*) + (f_B·*population B*)] with MO content. This trend is similar to the size obtained for the same aggregates containing DNA at CR (+/−) = 1.0, although in the lipoplexes the size distribution is unimodal.

Below CR (+/−) = 0.5, where Nile Red has not yet felt the DNA/cationic lipid assembly and restructuring, a more dispersive behavior for the systems with higher MO content is seen (Fig. 6A). This is in agreement with the size of the free liposomes (inset of Fig. 6B) and indicates that in this region there are mainly DODAB:MO structures coated with DNA [41], and the DNA compaction has not occurred yet. After this CR (+/−), the DNA-liposome surface interaction creates packing constraints and defects in the bilayers, triggering extensive interactions between adjacent bilayers. At this stage, clustering of the DNA coated DODAB:MO structures is expected to occur. This originates two opposing effects on light scattering intensity, as can be seen in Zimm equation (Eq. 14), which is valid for particles with size comparable to the wavelength of light [42]:

$$R_\theta = \frac{r^2}{V\left(1+\cos^2(2\theta)\right)} \times \left(\frac{I}{I_0}\right) = \frac{8\pi^4\alpha^2}{\lambda^4} \times N' \times \left(1 - \frac{16\pi^2 R_G^2 \sin^2(\theta)}{3\lambda^2}\right) \quad (14)$$

where (V) is the volume of solution under observation, (I/I_0) represents the fraction of scattered light at an angle of (2θ), (r) is the distance between the sample and the detector, (R_G) is particle's radius of gyration, (α) represents the particle polarizability which is related to the particle's volume and (N') is the number density of particles.

The concentration of scattering particles decreases as a result of clustering, whereas the size of the particles increases. From Eq. (14), it is deducible that the effect of particle enlargement upon clustering should originate an increase in light scattering. The clusters are intermediate structures that originate the final lamellar, hexagonal or inverted bicontinuous cubic structure-based lipoplexes. Along with this structure formation, the collapse of various liposomes also results in the release of their interior aqueous contents. If the condensed lipoplex has the same size as the liposome, a decrease of light scattering intensity is expected as a result of less number of particles. But if the lipoplexes are much larger than liposomes, the result is an increased light scattering.

The sudden increase of aggregate size seen in Fig. 6B near the charge neutralization point is probably a consequence of the above described clustering mechanism, and the subsequent decrease of aggregate size indicates the condensation and restructuring of the lipoplexes. From Fig. 6B, it is possible to conclude that, in systems with DODAB:MO (1:1 and 1:2), the DNA coated liposome clusters are sufficiently big to result in a peaked behavior in 90° SLS. This peaked behavior is less pronounced in the case of DODAB:MO (2:1), where only a slight decrease on scattered light intensity is observed. The different behavior of (2:1) system was already observed for CRs (+/−) < 0.5 in Fig. 3A, with the appearance of a red shift that changes the shape of Nile Red spectrum when compared to other DODAB molar ratios (1:1 and 1:2). This red shift was previously reported for the same lipid systems in the absence of DNA [25], where a highly dispersive region was documented for lower DODAB:MO concentrations.

Cryo-TEM micrographs of DNA/DODAB:MO (1:2) lipoplexes CR (+/−) = 4.0 are shown in Fig. 7. A further increase on MO content was performed, forming DNA/DODAB:MO (1:4), to better observe the effect of the *helper* lipid on the structures of the lipoplexes. By increasing the MO content from DNA/DODAB:MO (1:2) to (1:4), lipoplexes seem to preferentially adopt a non-lamellar phase with inverted structures identified previously as MO-rich domains. The superimposition of lamellar and inverted structures can be observed by the double pattern of the Fast Fourier Transform (FFT) profiles shown in Fig. 7. These MO-rich zones (depicted by the white arrows) become even more visible at DODAB:MO molar fractions higher than (1:2), where lipoplexes present a more globular and homogeneous shape/structure. The inter-lamellar distance measured on micrographs (6 nm for the highest MO content) is within the range of what has been determined in other MO enriched lipid systems containing DNA (5.5–6 nm) [20]. Therefore, in agreement with previously published SAXS analysis, the addition of DNA to positively charged membranes enriched with higher

Fig. 7. Cryo-TEM micrographs of DNA/DODAB:MO lipoplexes CR (+/−) = 4.0 (1 mM total lipid) prepared by one-step addition of cationic vesicles to DNA at 25 °C, complemented with Fast Fourier Transform (FFT) diagrams and gray-plot profiles for specified zones of the images, indicated with white dashed lines. White arrows indicate possible locations of MO-rich domains in the structures of the lipoplexes. A — DNA/DODAB:MO (1:2); B — DNA/DODAB:MO (1:4).

MO contents seems to exert a templating effect on the lyotropic phase, with the formation of non-lamellar phases (presumably inverted hexagonal phases), once fitting DNA in the inverted cubic phase (typical of MO) would incur in large energetic cost [20].

The information gathered with DLS, SLS and cryo-TEM suggests that the structure of the lipoplexes formed is dependent on the structure of the free DODAB:MO aggregates, that are dependent on the exact DODAB:MO molar fraction. A model representing the structure of the DODAB:MO DNA-lipoplexes is suggested in Fig. 8.

In DODAB-enriched formulations (DODAB:MO (4:1 and 2:1)), where lamellar liposomes are prevalent, the encapsulation of DNA will maintain the lamellar phase, and a multilamellar structure will predominantly be formed, with the anionic nucleic acids sandwiched between the lipid membranes. In MO-enriched formulations (DODAB:MO (1:1 and 1:2)), where a coexistence of lamellar and non-lamellar aggregates was observed [24], the encapsulation of DNA will originate a DODAB lamellar phase enclosing the MO non-lamellar phases, where the DNA will preferentially localize. Several biophysical studies [20,39,43,44] also support two possible models for the structure of lipoplexes, depending on the percentage of *helper* lipid.

Therefore, as represented in Fig. 8, distinct nanoscale structures of DNA-lipoplexes might be formed according to the DODAB:MO liposomes used to encapsulate the DNA: DNA/DODAB:MO (4:1, 2:1) lipoplexes exhibit a multilamellar organization with DNA filaments stacked between adjacent lipid bilayers while DNA/DODAB:MO (1:1 and 1:2) may bring about the coexistence of aggregates with lamellar and non-lamellar phases [19].

3.3. Effect of pH and anionic/neutral lipids on DNA dissociation from lipoplexes with different structure (lamellar/non-lamellar)

The level of lipoplex condensation and destabilization was also evaluated through FRET dependence on the relative distance between the DNA intercalating probe BOBO-1 and the lipid probe Rhodamine-DHPE (Fig. 9).

The addition of DODAB:MO cationic liposomes to DNA causes a linear increase of FRET efficiency with CR (+/−) until a plateau value is reached (Fig. 9A, B and C), where lipoplexes are formed and have its highest degree of compaction. The plateau value is reached at CR (+/−) = 2.0 for DNA/DODAB:MO (2:1) lipoplexes, CR (+/−) = 1.5 for DNA/DODAB:MO (1:1) lipoplexes and CR (+/−) = 1.0 for DNA/DODAB:MO (1:2) lipoplexes, which shows the fluidizing effect of MO within the lipoplex structure (already observed by Nile Red anisotropy measurements, Fig. 5), in agreement to the previously reported studies [19,23]. The final FRET efficiency (ϕ_{FRET}) obtained for all DNA/DODAB:MO lipoplexes at CR (+/−) = 4.0 shows a clear distinction between MO-rich formulations (1:2), with a ϕ_{FRET} of 90%, and DODAB-rich formulations (2:1), with a ϕ_{FRET} of 70%. The higher efficiency energy transfer for the MO-rich lipoplexes may reflect a close proximity between donor and acceptor, associated with the presence of a more fluid non-lamellar phase at higher MO contents (Fig. 8).

After cellular uptake via endocytosis, DNA lipoplexes must escape from endosomes so that DNA can progress toward the cell nucleus. Only a certain amount of time is available for this, since the endosomal pathway involves degradation of the endosome contents: initially through pH reduction and then through fusion with low pH lysosomes [5]. As the endosomal escape is known to be the main intracellular barrier for efficient cell transfection, it is interesting to evaluate the *in vitro* degree of lipoplex destabilization at relevant conditions such as: pH decrease (Fig. 9A′, B′ and C′) and interaction with anionic/neutral lipids (Fig. 9A″, B″ and C″). The initial pH decrease from 7.4 to 6.0 leads to a slight increase on the ionic strength of the medium, contributing to a higher compaction of all DNA/DODAB:MO lipoplexes prepared at CR (+/−) = 4.0. This compaction is noticed by the smooth increase on ϕ_{FRET} observed for all formulations. After this point, and until pH 4.0, a plateau is reached, followed by a decrease on ϕ_{FRET} that could be explained by some lipoplex degradation. This effect is less evident for lipoplexes with high MO content, due to their higher stability [19]. The stability of MO richer lipoplexes is probably due to the presence of non-lamellar MO phases (Fig. 8). These non-lamellar inverted phases together with the cationic charge conferred by DODAB allow improved entrapment of nucleic acids which are strongly confined within the aqueous domains of hexagonal cylinders stabilized by electrostatic bonds to DODAB positive charges and by hydrogen bonds with the water and MO headgroups. The same kind of rational has been proposed by other authors when explaining the confinement of DNA into MO enriched lipoplexes [45]. This stabilization effect makes the MO enriched formulations as more reliable for the encapsulation and protection of DNA assuring less lipoplex degradation inside the endosome. As a downside of the stability of the MO enriched lipoplexes is the DNA slow release, as such a strong confinement of the DNA at the water–lipid interface prevents its release into the excess water [45]. The interaction of DNA/DODAB:MO (2:1, 1:1 and 1:2) lipoplexes at CR(+/−) = 4.0 with the lipid surfactants OA, DOPA, DOPS and DOPE revealed that the uncharged phospholipid (DOPE) and the monovalent anionic phospholipids (DOPS) and (DOPA) poorly affect FRET efficiency, irrespective of the MO content in the lipoplexes. This suggests that the tested phospholipids have a limited influence on the lipoplex structure destabilization. Contrastingly, the fatty acid OA has a strong effect on the structural organization of DNA/DODAB:MO lipoplexes at a wide range of concentrations.

When up to 25 μM of OA concentration is added to DNA/DODAB:MO (2:1 and 1:1) lipoplexes, a decrease in ϕ_{FRET} occurs, indicating a destabilization of the lamellar phase of the lipoplexes, similar to the already observed for DODAB/OA mixed systems in the absence of DNA [46]. This destabilization occurs by the formation of planar bilayer fragments and the release of DNA from the lipoplex. For DNA/DODAB:MO (1:2 and 1:4) lipoplexes with the same OA concentration (25 μM), a slower and smaller $_{FRET}$ decrease is observed, suggesting a swelling of the lipoplex structure due to the diffusion of OA and a consequent stabilization of the inverted non-lamellar structures [47,48].

The gathered results suggest that the higher the MO content, the more stable the lipoplex, since the enriched MO lipoplex were more resistant to the degradation imposed by extreme pH conditions, and also to OA destabilization.

3.4. How lamellar versus inverted non-lamellar phases affect transfection efficiency of DNA/DODAB:MO lipoplexes

The structural variations discussed in the previous sections are reflected on the final transfection efficiency of DNA/DODAB:MO lipoplexes, as can be observed in Fig. 10.

Both non-lamellar and lamellar phases of the lipoplexes have an important role, and the balance between these two phases will be determinant for a more effective transfection. Lamellar phases can provide closer lipoplex–cell surface interaction, which is a crucial initial event for the lipoplex transfection [8]. Fig. 10 shows that DNA/DODAB:MO (2:1) was the most efficient lipoplex, with transfection efficiencies comparable to the commercial reagent Lipofectamine™ LTX when 1 μg DNA is used. These results are in agreement to the above considerations, reinforcing the advantage of having lipoplexes with a multilamellar organization that provide a tight membrane interaction between the lipoplex surface and the cellular membrane [8]. Nevertheless, the higher rigidity of this DODAB-rich lipid system results in a dose-effect response, meaning that a superior amount of lipid and DNA is needed to obtain transfection efficiencies comparable to Lipofectamine™ LTX.

Our results also demonstrate that the balance between lamellar and non-lamellar phases can be tuned using different MO content in the DODAB:MO lipoplexes. In this regard, the distribution of MO in the lipoplexes is determinant to understand the final transfection efficiency.

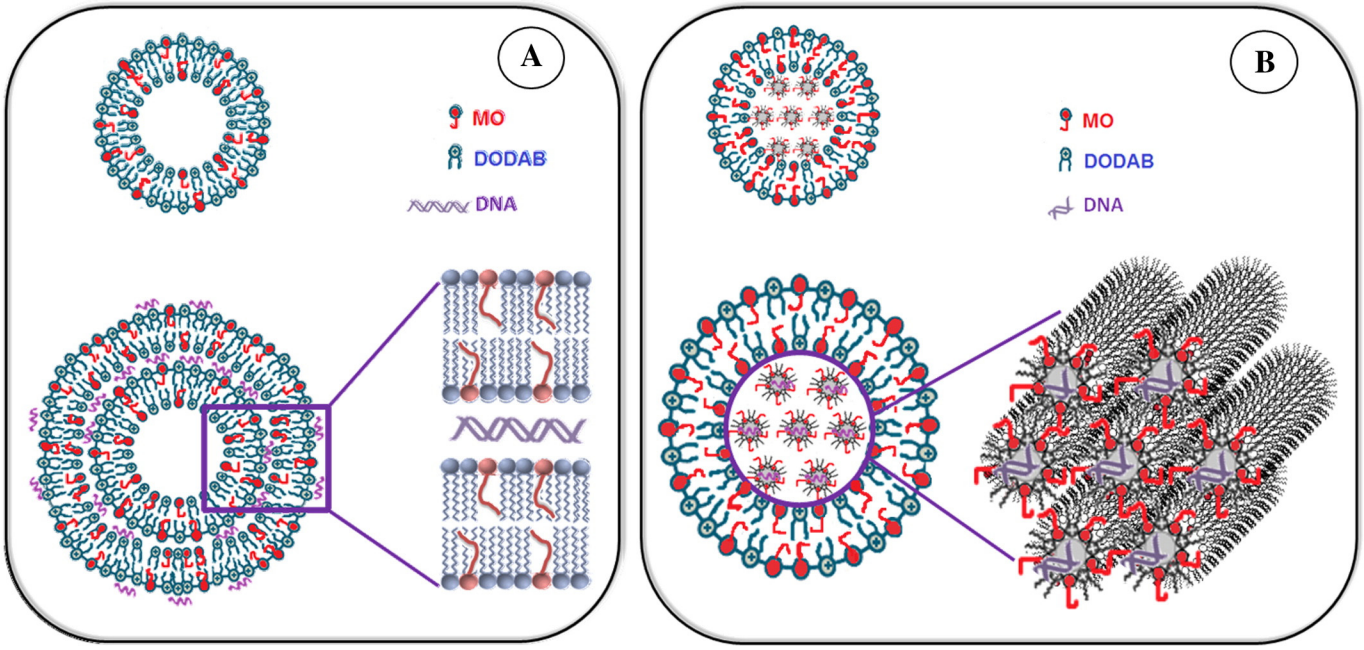

Fig. 8. Schematic representation of the proposed model for the structures of DODAB:MO liposomes (upper figure) and the correspondent DNA-lipoplexes (lower figure). (A) DODAB:MO (2:1) where the lamellar phase is predominant and MO is within the DODAB lamellar phase. (B) DODAB:MO (1:1 and 1:2) where MO organizes in inverted non-lamellar structures limited by DODAB lamellar phase.

Assuming a homogeneous distribution of DODAB and MO lipids, the membrane charge density (σ_M) [49] would be 0.008 e/Å^2 and 0.0051 e/Å^2 for DNA/DODAB:MO (1:2) and (1:4) lipoplexes respectively, compared with the already reported σ_M of 0.014 e/Å^2 and 0.010 e/Å^2 for DNA/DODAB:MO (2:1) and (1:1) lipoplexes [19]. However, these membrane charge densities do not agree with the zeta-potential measurements (data not shown), which indicates a non-homogeneous distribution of MO in the bilayers and corroborates the coexistence of several aggregates with different MO contents, as proposed in Fig. 8 [24]. Different coexistent phases (lamellar and inverted non-lamellar) have been reported to arise from cationic and helper lipids, resulting in a smaller transfection efficiency [8].

Higher MO content induces the formation of non-lamellar inverted domains with less hydration/microviscosity which are important features promoting lipoplex assembly and increasing DNA cooperative collapse. DNA is thus strongly confined in these MO domains, and consequently DNA/MO enriched lipoplexes are more stable and less prone to pH and anionic lipids destabilization. The sensitivity of the lipoplexes to OA destabilization is also dependent on MO, since lipoplexes with lower MO content are more destabilized by OA than lipoplexes with higher MO content. MO enriched formulations are thus more reliable for the encapsulation and protection of DNA assuring less lipoplex degradation inside the endosome. However, such an advantage in terms of stability does not translate in higher transfection rates of MO enriched lipoplexes. Indeed, in order to reach the levels of transfection efficiency obtained by the lipoplexes with multilamellar organization, the CR (+/−) must be increased. In the case of DNA/DODAB:MO (1:4) formulation, for example, increasing the CR (+/−) to 6.0 is enough to obtain transfection efficiencies comparable to Lipofectamine™ LTX (Fig. 10), without any significant increase in the associated cytotoxicity (data not shown). The explanation to the less efficient transfection is probably related with the higher stability conferred by the non-lamellar inverted phases (1:1, 1:2 and 1:4 formulations), that are advantageous regarding DNA protection, but have a drawback of hardening DNA release.

In general, MO as a helper lipid improves transfection efficiency by facilitating endosomal escape of DNA. However, our results indicate that high MO content causes less transfection when compared with DODAB richer lipoplexes (at CR ≤ 4.0). The distribution of MO in the DODAB:MO lipoplexes plays a determinant role in this matter. Nile Red probe senses the more fluidic environment of MO inverted non-lamellar domains of DODAB:MO (1:1 and 1:2) and the recent work corroborates the fluidity effect of increasing MO content by differential calorimetry studies [50]. It was expected that the higher fluidity of enriched MO lipoplexes would imply a higher fusogenicity of the particles, but MO is preferentially located inside of the lamellar DODAB structures, being less accessible to interact with the endosomes and promote fusion. In agreement to this assumption, it has been reported that MO-enriched liposomes (DODAB:MO (1:2)) did not promote a markedly fusogenic effect on endosome models compared to other systems with less MO (DODAB:MO (2:1)) [50]. Hence, the small fusogenic capacity associated with the tight DNA binding may justify the less transfection efficiency of MO enriched lipoplexes.

To sum up, formulations of DODAB containing MO as helper lipid present different properties and transfection efficiencies according to the MO content. Low MO contents have a similar gene silencing ability as the commonly used helper lipid 1,2-dioleyl-3-phosphatidylethanolamine (DOPE), but with much lower cytotoxicity [50]. Thus the introduction of MO as lipid helper is able to decrease the toxicity without compromising the efficiency of lipofection. Higher MO contents compromise the transfection efficiency that requires higher CR (+/−), but present the advantage of higher stability and possibility of co-encapsulation of drugs in MO enriched domains, providing a synergic drug/genetic therapy.

4. Conclusions

This work describes the effect of MO content on the structure and physicochemical properties of pDNA/DODAB:MO lipoplexes and establishes correlations with their transfection efficiency. The advantage of using MO as helper lipid is undeniable, as it is less toxic than other helper lipids like DOPE with similar gene silencing ability. However, increasing MO content at ratios of DODAB:MO equal or higher than 1:1 lowers the transfection efficiency. Therefore the content of MO can be tuned

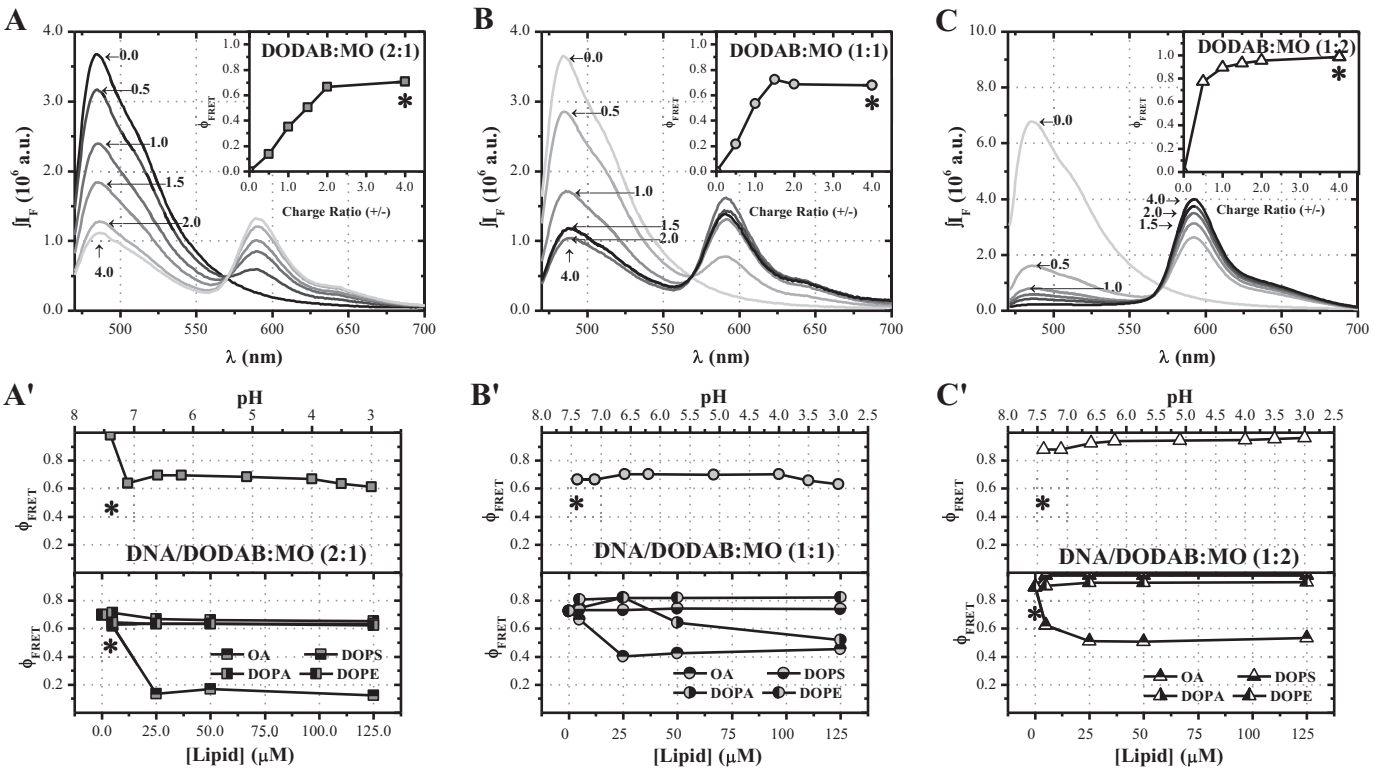

Fig. 9. Förster Resonance Energy Transfer (470–700 nm, $\lambda_{exc} = 460$ nm) of donor/acceptor pair BOBO-1/rhodamine-DHPE in DNA/DODAB:MO lipoplexes ([Phosphate] = 2 mM) at different charge ratios (+/−) (A, B, C, including their respective fluorescence spectra), upon incubation at different pHs and with different concentrations of neutral/anionic lipids (A′, B′, C′). Solid symbols represent the variation in the Förster resonance energy transfer efficiency (ϕ_{FRET}) calculated through Eq. (12) between BOBO-1 and rhodamine-DHPE species. The DNA intercalating probe BOBO-1 was used at probe/phosphate ratio of 1/200 and the lipid probe rhodamine-DHPE was used at probe/lipid ratio of 1/200. A — DNA/DODAB:MO (2:1) at different CRs (+/−); B — DNA/DODAB:MO (1:1) at different CRs (+/−); C — DNA/DODAB:MO (2:1) at different CRs (+/−); A′ — DNA/DODAB:MO (2:1) CR (+/−) = 4.0 at different pHs and different concentrations of anionic lipids; B′ — DNA/DODAB:MO (1:1) CR (+/−) = 4.0 at different pHs and different concentrations of anionic lipids; C′ — DNA/DODAB:MO (2:1) CR (+/−) = 4.0 at different pHs and different concentrations of anionic lipids.

according to the pretended application of the lipoplexes. If the researcher uses DODAB:MO systems with less content of MO it will achieve higher transfection rates and a controlled release of the nucleic acids, whereas the use of higher content of MO (DODAB:MO > (1:1)) requires higher CR (+/−) to reach the same transfection efficiency. Nonetheless, MO enriched systems still reach very acceptable transfection rates and they bear other advantages, such as an increased stability (preventing the immediate release of nucleic acid) and the possibility to co-encapsulate drugs in MO non-lamellar inverted domains providing a combined gene and drug therapy.

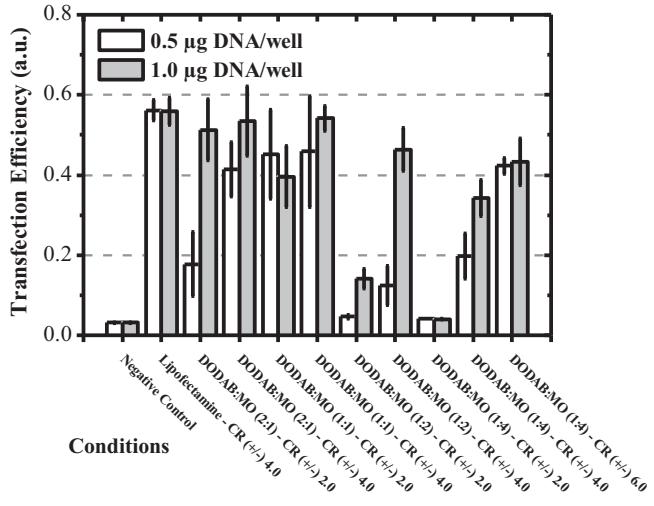

Fig. 10. Reporter β-galactosidase activity 48 h after transfection of 293T cells with different cationic lipoplexes (CRs (+/−) = 2.0, 4.0 and 6.0) prepared by one-step addition of cationic vesicles to pDNA (0.5 and 1.0 μg pDNA per well, white and light gray, respectively). Control: cells incubated with free pDNA. The mean (+/−) SD was obtained from three independent experiments.

Current ongoing strategies for the optimization of the MO-enriched systems are the inclusion of a third lipid which enhances DNA release without affecting the stability of the lipoplex structure.

Supplementary data to this article can be found online at http://dx.doi.org/10.1016/j.bbamem.2014.06.014.

Acknowledgements

We acknowledge Dr. David Gil from CIC-bioGUNE (Bizkaia Technology Park) for cryo-TEM measurements and Dra. Iva Pashkuleva from 3B's Research Group (AvePark Technology Park) for DLS and ζ-potential. This work has been funded by FEDER (037291) through POFC — COMPETE and by Portuguese funds from FCT through projects PTDC/QUI/69795/2006 (I&D grant), SFRH/BD/46968/2009 (PhD grant), PEst-C/BIA/UI4050/2011 (CBMA) and PEst-C/FIS/UI0607/2011 (CFUM). Marlene Lucio holds a position of Researcher FCT with the reference IF/00498/2012.

References

[1] N. Dan, D. Danino, Structure and kinetics of lipid-nucleic acid complexes, Adv. Colloid Interf. Sci. 205 (2014) 230–239.
[2] S. Misra, Human gene therapy — a brief overview of the genetic revolution, J. Assoc. Physicians India 61 (2013) 41–47.

[3] K.K. Ewert, A. Zidovska, A. Ahmad, N.F. Bouxsein, H.M. Evans, C.S. McAllister, C.E. Samuel, C.R. Safinya, Cationic lipid-nucleic acid complexes for gene delivery and silencing — pathways and mechanisms for plasmid DNA and siRNA, Top. Curr. Chem. 296 (2010) 191–226.
[4] K.K. Ewert, A. Ahmad, H.M. Evans, C.R. Safinya, Cationic lipid-DNA complexes for non-viral gene therapy — relating supramolecular structures to cellular pathways, Expert. Opin. Biol. Ther. 5 (2005) 33–53.
[5] A. Ahmad, H.M. Evans, K. Ewert, C.X. George, C.E. Samuel, C.R. Safinya, New multivalent cationic lipids reveal bell curve for transfection efficiency versus membrane charge density lipid-DNA complexes for gene delivery, J. Gene Med. 7 (2005) 739–748.
[6] K. Ewert, N.L. Slack, A. Ahmad, H.M. Evans, A.J. Lin, C.E. Samuel, C.R. Safinya, Cationic lipid-DNA complexes for gene therapy — understanding the relationship between complex structure and gene delivery pathways at the molecular level, Curr. Med. Chem. 11 (2004) 133–149.
[7] B. Ma, S. Zhang, H. Jiang, B. Zhao, H. Lv, Lipoplex morphologies and their influences on transfection efficiency in gene delivery, J. Control. Release 123 (2007) 184–194.
[8] L. Wasungu, D. Hoekstra, Cationic lipids, lipoplexes and intracellular delivery of genes, J. Control. Release 116 (2006) 255–264.
[9] X.X. Zhang, T.J. McIntosh, M.W. Grinstaff, Functional lipids and lipoplexes for improved gene delivery, Biochimie 94 (2012) 42–58.
[10] T. Wang, J.R. Upponi, V.P. Torchilin, Design of multifunctional non-viral gene vectors to overcome physiological barriers: dilemmas and strategies, Int. J. Pharm. 427 (2012) 3–20.
[11] D. Hirsch-Lerner, M. Zhang, H. Eliyahu, M.E. Ferrari, C.J. Wheeler, Y. Barenholz, Effect of "helper" 'lipid' on lipoplex electrostatics, Biochim. Biophys. Acta 1714 (2005) 71–84.
[12] S.W. Hui, M. Langner, Y. Zhao, P. Ross, E. Hurley, K. Chan, The role of helper lipids in cationic liposome-mediated gene transfer, Biophys. J. 71 (1996) 590–599.
[13] S. Mochizuki, N. Kanegae, K. Nishina, Y. Kamikawa, K. Koiwai, H. Masunaga, K. Sakurai, The role of the helper lipid dioleoylphosphatidylethanolamine (DOPE) for DNA transfection, Biochim. Biophys. Acta 1828 (2012) 412–418.
[14] D. Pozzi, C. Marchini, F. Cardarelli, H. Amenitsch, C. Garulli, A. Bifone, G. Caracciolo, Transfection efficiency boost of cholesterol-containing lipoplexes, Biochim. Biophys. Acta 1818 (2012) 2335–2343.
[15] I. Koltover, T. Salditt, J.O. Radler, C.R. Safinya, An inverted hexagonal phase of cationic liposome-DNA complexes related to DNA release and delivery, Science 3 (1998) 78–81.
[16] I.S. Zuhorn, V. Oberle, W.H. Visser, J.B.F.N. Engberts, U. Bakowsky, E. Polushkin, D. Hoekstra, Phase behavior of cationic amphiphiles and their mixtures with helper lipids, Biophys. J. 83 (2002) 2096–2108.
[17] R. Koynova, B. Tenchov, Cationic lipids: molecular structure/transfection activity relationships and interactions with biomembranes, Top. Curr. Chem. 296 (2010) 51–93.
[18] R. Koynova, L. Wang, R.C. MacDonald, Cationic phospholipids forming cubic phases — lipoplex structure and transfection efficiency, Mol. Pharm. 5 (2008) 739–744.
[19] J.P.N. Silva, A.C.N. Oliveira, M.P.P.A. Casal, A.F.C. Gomes, P.J.G. Coutinho, O.M.F.P. Coutinho, M.E.C.D.R. Oliveira, DODAB:monoolein-based lipoplexes as non-viral vectors for transfection of mammalian cells, Biochim. Biophys. Acta 1808 (2011) 2440–2449.
[20] C. Leal, K.K. Ewert, N.F. Bouxsein, R.S. Shirazi, Y. Li, C.R. Safinya, Stacking of short DNA induces the gyroid cubic-to-inverted hexagonal phase transition in lipid-DNA complexes, Soft Matter 9 (2013) 795–804.
[21] R. Koynova, Y.S. Tarahovsky, L. Wang, R.C. MacDonald, Lipoplex formulation of superior efficacy exhibits high surface activity and fusogenicity, and readily releases DNA, Biochim. Biophys. Acta 1768 (2007) 375–386.
[22] R. Koynova, L. Wang, R.C. MacDonald, An intracellular lamellar-nonlamellar phase transition rationalizes the superior performance of some cationic lipid transfection agents, Proc. Natl. Acad. Sci. U. S. A. 103 (2006) 14373–14378.
[23] J.P.N. Silva, A.C.N. Oliveira, A.C. Gomes, M.E.C.D.R. Oliveira, Development of DODAB-MO Liposomes for Gene Delivery, in: InTech (Ed.), Cell Interaction, Rijeka, Croatia, 2012, pp. 245–272.
[24] I.M.S.C. Oliveira, J.P.N. Silva, E. Feitosa, E.F. Marques, E.M.S. Castanheira, M.E.C.D.R. Oliveira, Aggregation behavior of aqueous dioctadecyldimethylammonium bromide/monoolein mixtures: a multitechnique investigation on the influence of composition and temperature, J. Colloid Interface Sci. 374 (2012) 206–217.
[25] J.P.N. Silva, P.J.G. Coutinho, M.E.C.D.R. Oliveira, Characterization of mixed DODAB-monoolein aggregates using Nile Red as a solvatochromic and anisotropy fluorescent probe, J. Photochem. Photobiol. A Chem. 203 (2009) 32–39.
[26] F.H. Stephenson, Calculations for Molecular Biology and Biotechnology, 1st ed. Academic press, Elsevier, New York (USA), 2003.
[27] M.M.G. Krishna, Excited-state kinetics of the hydrophobic probe Nile Red in membranes and micelles, J. Phys. Chem. A 103 (1999) 3589–3595.
[28] A. Cser, K. Nagy, L. Biczok, Fluorescence lifetime of Nile Red as a probe for the hydrogen bonding strength with its microenvironment, Chem. Phys. Lett. 360 (2002) 473–478.
[29] P.J.G. Coutinho, E.M.S. Castanheira, M.C. Rei, M.E.C.D. Real-Oliveira, Nile Red and DCM fluorescence anisotropy studies in C12E7DPPC mixed systems, J. Phys. Chem. B 106 (2002) 12841–12846.
[30] T. Förster, Zwischenmolekulare energiewanderung und fluoreszenz, Ann. Phys. 437 (1948) 55–75.
[31] H. Sahoo, Förster resonance energy transfer – a spectroscopic nanoruler – principle and applications, J. Photochem. Photobiol. C 12 (2011) 20–30.
[32] V.A. Rakhmanova, R.C. MacDonald, A microplate fluorimetric assay for transfection of the β-galactosidase reporter gene, Anal. Biochem. 257 (1998) 234–237.
[33] G. Hungerford, E.M.S. Castanheira, A.L.F. Baptista, P.J.G. Coutinho, M.E.C.D. Real-Oliveira, Domain formation in DODAB-cholesterol mixed systems monitored via Nile Red anisotropy, J. Fluoresc. 15 (2005) 835–840.
[34] S. May, A. Ben-Shaul, Modeling Of cationic lipid-DNA complexes, Curr. Med. Chem. 11 (2004) 151–167.
[35] D. Hirsch-Lerner, Y. Barenholz, Hydration of lipoplexes commonly used in gene delivery — follow-up by Laurdan fluorescence changes and quantification by differential scanning calorimetry, Biochim. Biophys. Acta 1461 (1999) 47–57.
[36] M. Muñoz-Úbeda, A. Rodríguez-Pulido, A. Nogales, A. Martín-Molina, E. Aicart, E. Junquera, Effect of lipid composition on the structure and theoretical phase diagrams of DC-Chol/DOPE-DNA lipoplexes, Biomacromolecules 11 (2010) 3332–3340.
[37] A.E. Regelin, S. Fankhaenel, L. Gurtesch, C. Prinz, G. Kiedrowski, U. Massing, Biophysical and lipofection studies of DOTAP analogs, Biochim. Biophys. Acta 1464 (2000) 151–164.
[38] S. Choosakoonkriang, C.M. Wiethoff, T.J. Anchordoquy, G.S. Koe, J.G. Smith, C.R. Middaugh, Infrared spectroscopic characterization of the interaction of cationic lipids with plasmid DNA, J. Biol. Chem. 276 (2001) 8037–8043.
[39] C. Leal, D. Sandström, P. Nevsten, D. Topgaard, Local and translational dynamics in DNA-lipid assemblies monitored by solid-state and diffusion NMR, Biochim. Biophys. Acta 1778 (2008) 214–228.
[40] P. Taboada, D. Attwood, J.M. Ruso, M. Garcia, V. Mosquera, Static and dynamic light scattering study on the association of some antidepressants in aqueous electrolyte solutions, Phys. Chem. Chem. Phys. 2 (2000) 5175–5179.
[41] M.T. Kennedy, E.V. Pozharski, V.A. Rakhmanova, R.C. MacDonald, Factors governing the assembly of cationic phospholipid-DNA complexes, Biophys. J. 78 (2000) 1620–1633.
[42] C.R. Cantor, P.R. Schimell, Biophysical Chemistry – Part II – Techniques for the Study of Biological Structure and Function, 1st ed. W.H. Freeman, New York (USA), 1980.
[43] C. Leal, N.F. Bouxsein, K.K. Ewert, C.R. Safinya, Highly efficient gene silencing activity of siRNA embedded in a nanostructured gyroid cubic lipid matrix, J. Am. Chem. Soc. 132 (2010) 16841–16847.
[44] A. Bilalov, J. Elsing, E. Haas, C. Schmidt, U. Olsson, Embedding DNA in surfactant mesophases — the phase diagram of the ternary system dodecyltrimethylammonium-DNA-monoolein-water in comparison to the DNA-free analogue, J. Colloid Interface Sci. 394 (2013) 360–367.
[45] I. Amar-Yuli, J. Adamcik, S. Blau, A. Aserin, N. Garti, R. Mezzenga, Controlled embedment and release of DNA from lipidic reverse columnar hexagonal mesophases, Soft Matter 7 (2011) 8162–8168.
[46] M. Kepczynski, J. Lewandowska, K. Witkowska, S. Kedracka-Krok, V. Mistrikovac, J. Bednarc, P. Wydro, M. Nowakowska, Bilayer structures in dioctadecyldimethylammonium bromide-oleic acid dispersions, Chem. Phys. Lipids 164 (2011) 359–367.
[47] D.A. Ferreira, M.V.L.B. Bentley, G. Karlsson, K. Edwards, Cryo-TEM investigation of phase behaviour and aggregate structure in dilute dispersions of monoolein and oleic acid, Int. J. Pharm. 310 (2006) 203–212.
[48] Y. Aota-Nakano, S.J. Li, M. Yamazaki, Effects of electrostatic interaction on the phase stability and structures of cubic phases of monoolein-oleic acid mixture membranes, Biochim. Biophys. Acta 1461 (1999) 96–102.
[49] A.J. Lin, N.L. Slack, A. Ahmad, C.X. George, C.E. Samuel, C.R. Safinya, Three-dimensional imaging of lipid gene-carriers membrane charge density controls universal transfection behavior in lamellar cationic liposome-DNA complexes, Biophys. J. 84 (2003) 3307–3316.
[50] A.C. Oliveira, T.F. Martens, K. Raemdonck, R.D. Adati, E. Feitosa, C. Botelho, A.C. Gomes, K. Braeckmans, M.E.R. Oliveira, Dioctadecyldimethylammonium-monoolein nanocarriers for efficient in vitro gene silencing, ACS Appl. Mater. Interfaces 6 (9) (2014) 6977–6989.